JACS
JOURNAL OF THE AMERICAN CHEMICAL SOCIETY
Article
pubs.acs.org/JACS

Quantum Mechanical/Molecular Mechanical Study on the Mechanism of the Enzymatic Baeyer–Villiger Reaction

Iakov Polyak,[†] Manfred T. Reetz,[†,‡] and Walter Thiel*[,†]

[†]Max-Planck-Institut für Kohlenforschung, Kaiser-Wilhelm-Platz 1, D-45470 Mülheim an der Ruhr, Germany
[‡]Fachbereich Chemie, Philipps-Universität Marburg, Hans-Meerwein-Strasse, D-35032 Marburg, Germany

Supporting Information

ABSTRACT: We report a combined quantum mechanical/molecular mechanical (QM/MM) study on the mechanism of the enzymatic Baeyer–Villiger reaction catalyzed by cyclohexanone monooxygenase (CHMO). In QM/MM geometry optimizations and reaction path calculations, density functional theory (B3LYP/TZVP) is used to describe the QM region consisting of the substrate (cyclohexanone), the isoalloxazine ring of C4a-peroxyflavin, the side chain of Arg-329, and the nicotinamide ring and the adjacent ribose of $NADP^+$, while the remainder of the enzyme is represented by the CHARMM force field. QM/MM molecular dynamics simulations and free energy calculations at the semiempirical OM3/CHARMM level employ the same QM/MM partitioning. According to the QM/MM calculations, the enzyme–reactant complex contains an anionic deprotonated C4a-peroxyflavin that is stabilized by strong hydrogen bonds with the Arg-329 residue and the $NADP^+$ cofactor. The CHMO-catalyzed reaction proceeds via a Criegee intermediate having pronounced anionic character. The initial addition reaction has to overcome an energy barrier of about 9 kcal/mol. The formed Criegee intermediate occupies a shallow minimum on the QM/MM potential energy surface and can undergo fragmentation to the lactone product by surmounting a second energy barrier of about 7 kcal/mol. The transition state for the latter migration step is the highest point on the QM/MM energy profile. Gas-phase reoptimizations of the QM region lead to higher barriers and confirm the crucial role of the Arg-329 residue and the $NADP^+$ cofactor for the catalytic efficiency of CHMO. QM/MM calculations for the CHMO-catalyzed oxidation of 4-methylcyclohexanone reproduce and rationalize the experimentally observed (*S*)-enantioselectivity for this substrate, which is governed by the conformational preferences of the corresponding Criegee intermediate and the subsequent transition state for the migration step.

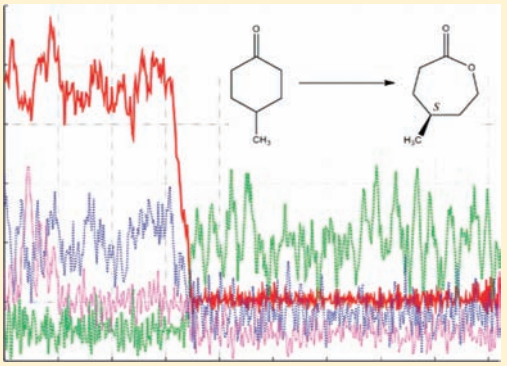

1. INTRODUCTION

The Baeyer–Villiger (B–V) oxidation[1] transforms ketones into esters or lactones using stoichiometric amounts of hydrogen peroxide, peracids, or alkylhydroperoxides. The reaction is catalyzed by acids, bases, or transition metals, asymmetric versions being possible by the use of chiral transition metal catalysts[2] or organocatalysts.[3] Unfortunately, notable activity and high enantioselectivity is restricted to the reaction of strained cyclic ketones such as cyclobutanone derivatives. An attractive alternative is the O_2-driven enzymatic variant that is catalyzed by Baeyer–Villiger monooxygenases (BVMOs).[4] These enzymes have proven to be of great interest for synthetic chemists[4,5] because in many cases their use allows stereoselective access to valuable products such as chiral lactones without the need for hazardous reagents, with only water as an ecologically benign byproduct. In those cases in which a given substrate fails to react stereoselectively, directed evolution[6] can be employed as a tool to control this important catalytic parameter.[7,8] A variety of different BVMOs have been isolated, characterized, and used in synthetic organic chemistry, cyclohexanone monooxygenases (CHMOs) forming an important sub-family with CHMO from *Acinetobacter* sp. NCIMB 9871 (EC 1.14.13.22) as the most prominent member.[9]

The reaction mechanism of BVMOs (see Figure 1) has been explored with the use of kinetic and spectroscopic methods.[10−13] In the initial phase of the reaction, the enzyme-bound FAD cofactor is reduced by NADPH via hydride transfer. The reduced $FADH^-$ then interacts with an oxygen molecule and forms the C4a-peroxyflavin intermediate ($FADHOO^-$). Up to this point, the reaction can proceed without the substrate necessarily occupying the binding site. For CHMO it was shown[11] that the C4a-peroxyflavin is stable for some time, but in the absence of substrate it slowly transforms into the protonated state, C4a-hydroperoxyflavin (pK_a = 8.4), which was found to be unreactive. In the presence of substrate, the B–V reaction takes place: the consensus view is that a tetrahedral Criegee intermediate is formed, which subsequently fragments with concomitant C-migration to give C4a-hydroxyflavin and a product (ester or lactone). The FAD cofactor in its oxidized form is then recovered by the

Received: November 4, 2011
Published: January 5, 2012

   dx.doi.org/10.1021/ja2103839 | *J. Am. Chem.Soc.* 2012, 134, 2732–2741

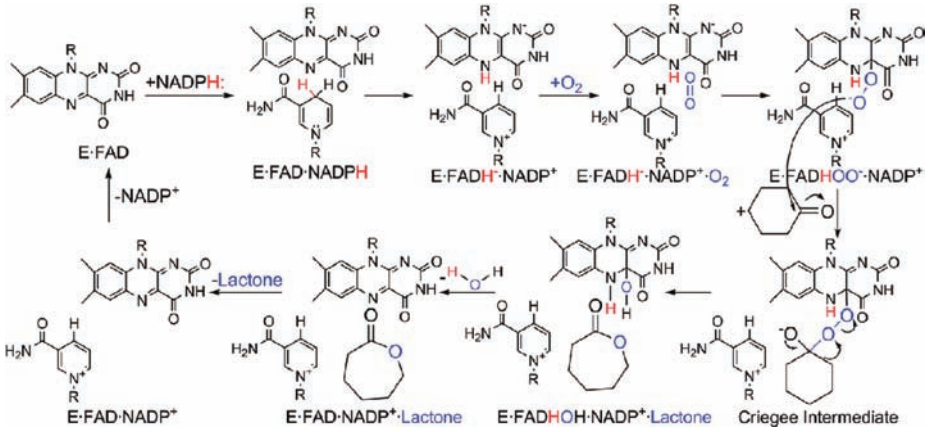

Figure 1. Mechanism of CHMO reaction. Reproduced with permission from ref 14. Copyright 2009 American Chemical Society.

spontaneous elimination of a water molecule. Furthermore, the initially formed $NADP^+$ needs to be released, and a new NADPH cofactor must bind to the enzyme in order to reduce FAD into the catalytically active form before the next reaction cycle can begin. The $NADP^+$ cofactor is considered to play an important role in stabilizing the C4a-peroxyflavin, and the Arg-329 residue is vital for the B–V reaction to proceed,[12] presumably by stabilizing the Criegee intermediate.

Nonenzymatic B–V reactions in synthetic organic chemistry proceed by two steps, both of which also occur in the enzymatic variant (Figure 1).[15,16] In the addition step, the peroxy moiety of an oxidant such as an alkylhydroperoxide attacks the carbonyl carbon of the ketone to generate the so-called Criegee intermediate. In the following migration step, one of the C–C σ bonds adjacent to the carbonyl carbon migrates to the closest oxygen atom of the peroxy group, with the O–O bond being simultaneously cleaved. The so-called anti-periplanar arrangement is part of the stereoelectronic requirement for the reaction to proceed smoothly, leading to the formation of either an ester or a lactone. In solution, the B–V reaction is generally carried out in an acidic environment so that the carbonyl oxygen is protonated during the addition step and loses its proton during or immediately after the migration step. However, base-catalyzed reactions have also been reported,[16] which are believed to proceed via an anionic Criegee intermediate. Whether the addition or migration (fragmentation) step is rate-determining will depend both on the type of the substrate and the reaction environment.[15]

The nonenzymatic B–V reaction has been studied computationally for small molecules in the gas phase and in solution.[17] In the case of the acid-catalyzed B–V oxidation of cyclohexanone,[17d] the migration step was found to be rate-determining, and the overall reaction was highly exothermic (by −67.4 kcal/mol). To our knowledge, the enzyme-catalyzed B–V reaction has not been studied theoretically up to now.

The first X-ray structure of a BVMO was that of phenyl acetone monooxygenase (PAMO) with bound FAD but in the absence of the flavin cofactor and lacking a substrate.[18] The first crystal structure of a BVMO enzyme that contains both FAD and $NADP^+$ cofactors bound to the enzyme was reported for the CHMO from *Rhodococcus* sp. strain HI-31 by Lau, Berghuis, and co-workers.[14] It has no ligand or inhibitor in the binding site. One of the two structures resolved for this CHMO (the "closed" form) was considered to represent the conformation of the enzyme that is best suited for the formation of the Criegee intermediate and the subsequent fragmentation. CHMO from *Rhodococcus* sp. strain HI-31 and CHMO from *Acinetobacter* sp. NCIMB 9871 are homologous BVMOs, sharing an overall 55% sequence identity.[14] The two enzymes display similar profiles with respect to the sense and degree of stereoselectivity, as for example in the desymmetrization of 4-methylcyclohexanone (**1**), both BVMOs leading to >96% ee in favor of the respective (*S*)-lactone (**2**) (Figure 2).

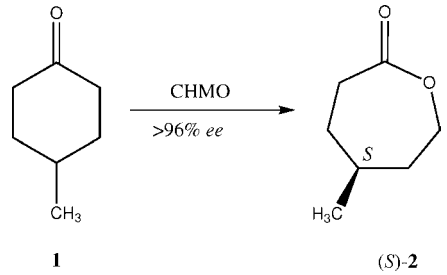

Figure 2. Stereochemical conversion of 4-methylcyclohexanone (**1**) to (*S*)-4-methyl-ε-caprolactone ((*S*)-**2**) in the B–V reaction catalyzed by CHMO.

According to phylogenetic analysis, the sequence of CHMO (*Rhodococcus*) clusters with several other CHMOs as well, showing that it is a good representative of this family of BVMOs.[14] Therefore, the crystal structure of the closed form of CHMO (*Rhodococcus*), hereafter referred to as CHMO, was used as the starting point for our investigation. More recently, further X-ray structures have become available for PAMO (and some PAMO mutants) containing both FAD and $NADP^+$ cofactors, including those for the reduced form of PAMO without and with a bound 2-(*N*-morpholino)ethanesulfonic acid (MES) inhibitor.[13]

In this article, we report quantum mechanical/molecular mechanical (QM/MM) calculations on the B–V oxidation of cyclohexanone in the active site of CHMO. Our aim is to provide a detailed atomistic understanding of the mechanism of this enzymatic reaction starting from the substrate-enzyme complex and up to the formation of the product (ε-caprolactone). Another important goal is to find an explanation of the observed enantioselectivity of CHMO as a catalyst in the desymmetrization of **1** on the basis of the computed structures for the Criegee intermediate and the subsequent transition state.

dx.doi.org/10.1021/ja2103839 | *J. Am. Chem.Soc.* 2012, 134, 2732–2741

2. METHODS

Initial coordinates were taken from the X-ray structure of CHMO from *Rhodococcus* sp. strain HI-31 (PDB code 3GWD, resolution 2.3 Å).[14] The protonation states of the titratable residues (His, Glu, Asp) were chosen on the basis of the pK_a values obtained via the H^{++} Web software[19] and the PROPKA procedure[20] and were verified through visual inspection. Based on the FAD structure in the crystal, the FADHOO$^-$ geometry was built and optimized in the gas phase with all coordinates frozen, except for those of the peroxy group oxygen atoms and the C4a carbon atom of the isoalloxazine ring which is directly bound to the peroxy group. The whole enzyme was solvated in a water ball of 45 Å radius centered at the CHMO center of mass. The total charge of the whole system was $-30e$ at this point; to avoid artifacts, it was neutralized by Mg^{2+} and Cl^- ions via random substitution of solvent water molecules lying at least 5.5 Å away from any protein atom. In molecular dynamics (MD) simulations, a potential was imposed on the water sphere to prevent the outer solvent water molecules from drifting away into the vacuum.

The solvated system was relaxed via energy minimization and subjected to MD simulations at the MM level using the CHARMM22 force field[21] as implemented within the CHARMM program.[22] During the classical energy minimizations and MD simulations, the whole system was moving freely except for the FADHOO$^-$ and NADP$^+$ cofactors, the coordinates of which were kept fixed at the positions of the crystal structure. A random snapshot from the classical MD trajectory was used as starting point for the QM/MM calculations.

Cyclohexanone was docked into the enzyme active site of the chosen snapshot via the AutoDock program.[23] The water molecules overlapping with the docked ligand were deleted as well as the two water molecules close to the distal oxygen of the FADHOO$^-$ peroxy group. The resulting system (see Figure 3) contained 39 913 atoms.

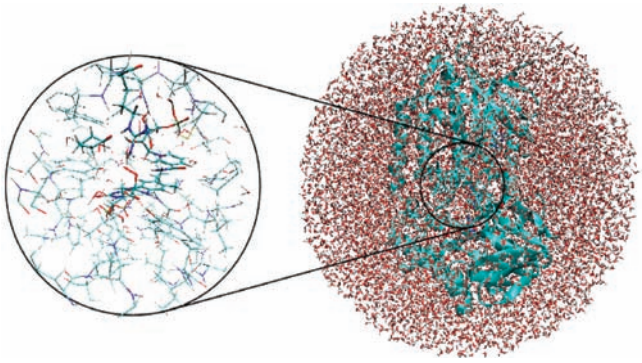

Figure 3. System used for QM/MM calculations. The active region is enlarged (on the left).

The chosen QM/MM methodology[24,25] is analogous to that used in previous studies from our group. Here we mention only the aspects relevant to the present work. In the QM/MM calculations, the QM part was treated by density functional theory (DFT) using the B3LYP functional,[26] while the MM part was described by the CHARMM22 force field. An electronic embedding scheme[27] was adopted in the QM/MM calculations, with the MM point charges being incorporated into the one-electron Hamiltonian during the QM calculation. No cutoffs were introduced for the nonbonding MM and QM/MM interactions. Hydrogen link atoms with the charge shift model[28] were employed to treat the QM/MM boundary. The QM/MM calculations were performed with the ChemShell package[29] using the TURBOMOLE program[30] to obtain the energy and gradients for the QM part and the DL_POLY program[31] to compute the energy and gradients of the MM part represented by the CHARMM22 force field. Within ChemShell, the HDLCopt[32] and DL_FIND[33] optimizers were used as well as the MD module.

The QM region incorporated all atoms from the isoalloxazine ring of C4a-peroxyflavin, cyclohexanone, the side chain of Arg-329, and the nicotinamide ring and the adjacent ribose of NADP$^+$. The latter group was included in the QM region upon inspection of preliminary optimization results with a smaller QM region, which placed the ribose 2′-hydroxyl group into close proximity to the oxygen atom of cyclohexanone. The total charge of the QM region was +1.

The SVP basis set[34] was chosen for initial B3LYP/CHARMM pathway explorations and geometry optimizations. The stationary points thus obtained along the reaction path were reoptimized using the TZVP basis set[35] in B3LYP/CHARMM calculations. Empirical dispersion corrections for DFT[36] (DFT-D2) were applied in single-point calculations at the B3LYP/TZVP level to check for the influence of dispersion. Additional single-point calculations were carried out at the M06-2X/TZVP level for further validation using a modern functional that performs particularly well for main-group thermochemistry and kinetics.[37]

During the QM/MM geometry optimizations, the active region to be optimized (see Figure 3) included all QM atoms as well as all residues and water molecules of the MM region within 12 Å of the C4a atom in the isoalloxazine ring of FADHOO$^-$. This radius was chosen such that all enzyme residues around the binding pocket were part of the active region.

Reaction paths were scanned along suitably defined reaction coordinates by performing sequences of restrained optimizations. The resulting structures served as starting points for subsequent full optimizations of the relevant stationary points. Energy minimizations and transition state (TS) searches were done with the low-memory Broyden–Fletcher–Goldfarb–Shanno (L-BFGS) algorithm[38] and with the microiterative TS optimizer that combines L-BFGS and the partitioned rational function optimizer[39] (P-RFO), both of which are implemented in the HDLCopt module of ChemShell. Frequency calculations were performed for the QM region to confirm that the optimized TS structure is indeed characterized by one imaginary frequency and a suitable transition vector, and subsequent intrinsic reaction coordinate calculations ensured that the TS is indeed connected to the proper minima by a continuous pathway.

QM/MM dynamics was performed with the use of the dynamics module within ChemShell. These MD simulations employed the NVT ensemble with a Nosé-Hoover thermostat.[40] The QM part of the system was treated with the OM3 semiempirical method[41] in these QM/MM MD runs; the active region was the same as in the QM/MM optimizations (see above), with all other atomic coordinates being frozen. The SHAKE procedure[42] was applied at every step for the water O–H bonds. QM/MM free energy calculations were carried out at the OM3/CHARMM level using thermodynamic integration and established procedures described elsewhere.[43]

For the purpose of comparison, pure QM calculations were performed at the B3LYP/TZVP level in the gas phase for the QM region (including link atoms), which was "anchored" in space by freezing the Cartesian coordinates of all atoms that were covalently bound to MM atoms. In this way, all three minima along the reaction path were reoptimized, potential energy scans were carried out along the reaction coordinates for addition and migration, and the TS for the migration step was also reoptimized.

3. RESULTS AND DISCUSSION

In the crystal structure determination of CHMO,[14] two structures were resolved. It was argued that one of these, namely the "closed" structure, is likely to represent the enzyme conformation in the post-flavin reduction state and during the essential chemical transformations.[14] For the current mechanistic investigation, this "closed" structure was chosen as the starting point. Binding of an oxygen molecule to FAD will hardly cause significant conformational changes in the active site, and it is known experimentally[11] that the enzyme remains stable after oxygen binding in the absence of a substrate in the binding pocket. Therefore, the crystal structure was manually modified by adding a peroxy group to the FAD cofactor and subjected to MD equilibration (after adding solvent molecules and counterions, see above). Cyclohexanone was then docked

dx.doi.org/10.1021/ja2103839 | J. Am. Chem.Soc. 2012, 134, 2732–2741

into the binding site of a snapshot taken from the sampling MD trajectory, followed by an energy minimization to adjust the orientation of cyclohexanone and the active-site residues. This procedure is based on the assumption that substrate binding does not cause a significant change in the overall protein structure and, in particular, in the orientation of the $FADHOO^-$ and $NADP^+$ cofactors.

The "closed" crystal structure contains two water molecules in the region where the oxygen molecule is bound, which can form hydrogen bonds with the distal oxygen of the $FADHOO^-$ peroxy group after the latter is inserted manually (see above). Preliminary scans along the reaction coordinate for the addition step indicated that these two water molecules destabilize the forming Criegee intermediate: if they are included in the QM region, the Criegee intermediate dissociates spontaneously after releasing the reaction coordinate restraints in a full optimization. Therefore, these two water molecules were removed from the system, and the reaction mechanism was investigated under the assumption that specific water molecules are not directly involved.

The chosen setup for CHMO is supported by recently published X-ray structures of another BVMO enzyme, namely PAMO containing $NADP^+$ and FAD in its oxidized form (PDB code 2YLR), in its reduced form (PDB code 2YLS), and with a bound MES inhibitor (PDB code 2YLT).[13] After alignment, the three structures match very well, with root-mean-square deviations for the protein backbone atoms (residues 12−542) of only 0.281 (2YLR vs 2YLS), 0.283 (2YLR vs 2YLT), and 0.322 Å (2YLS vs 2YLT). Visual inspection confirms that there are no significant conformational changes upon binding of MES to PAMO. Furthermore, the PAMO crystal structures without bound MES contain water molecules close to the FAD isoalloxazine ring which are absent in the structure with MES, indicating that inhibitor or substrate binding may indeed lead to the removal of water molecules from the active site of BVMO enzymes.

The structure obtained by our setup procedure for CHMO was subjected to QM/MM geometry optimization. The resulting reactant complex is shown in Figure 4, featuring cyclohexanone in the chair conformation in a well-defined position in the binding pocket, with hydrogen bonds between the carbonyl oxygen atom and Arg-329 and the $NADP^+$ ribose 2′-hydroxyl group (NADP:HN2T) (Table 1). The molecule can also be positioned in a different way, namely in a juxtaposition resulting from rotation by 180° around the main axis passing through the CYHN:C1 and CYHN:C4 atoms. The resulting geometry was reoptimized at the QM(B3LYP/SVP)/CHARMM level. During this minimization, cyclohexanone retained its new orientation and did not rotate back, but the total energy of the optimized minimum structure (Supporting Information (SI), Figure S1) was 11 kcal/mol higher than that of the previously optimized complex with cyclohexanone in its original orientation. In addition, we checked the energy required for converting the favored reactant complex (Figure 4) into the alternative binding mode by constrained potential energy scans at the OM3/CHARMM level: the resulting barrier for rotation of the cyclohexanone moiety around the C1−C4 axis is more than 25 kcal/mol and thus prohibitively high in the enzyme environment. As delineated later (section 3.5), these findings are the key to explaining the source of enantioselectivity in the B−V reaction of **1**.

The mechanistic studies at the QM/MM level started from the enzyme−reactant complex. The energy values and

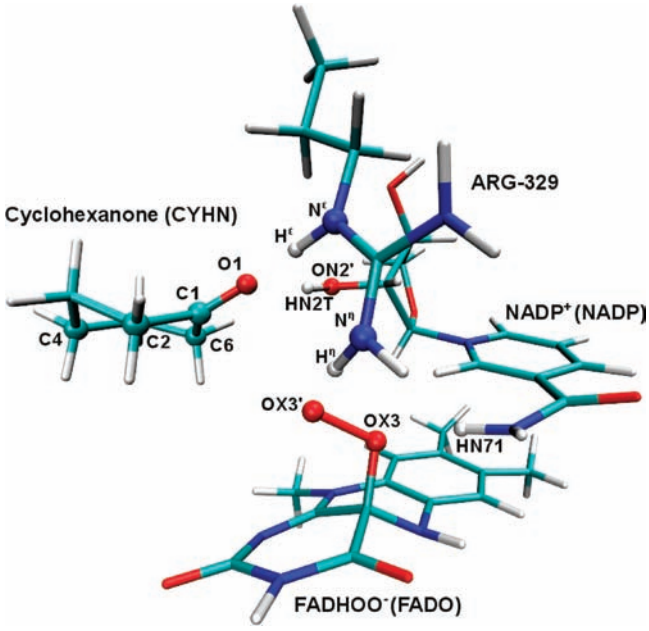

Figure 4. Enzyme−reactant complex (QM region only) optimized at the QM(B3LYP/TZVP)/CHARMM level with definition of atom labels used in the text. Residue names are given in parentheses. For characteristic interatomic distances, see text and Table 1.

Table 1. Characteristic Interatomic Distances in QM(B3LYP/TZVP)/CHARMM Optimized Geometries (in Å)[a]

	reactant	intermediate	TS2	product
CYHN:C1-FADO:OX3′	3.41	1.61	1.38	1.32
CYHN:O1-Arg329:H^{ε}	1.91	1.60	1.62	1.75
CYHN:O1-NADP:HN2T	1.77	1.53	1.58	1.69
FADO:OX3′-Arg329:$H^{\eta l}$	1.57	1.98	1.97	3.46
FADO:OX3-NADP:HN71	1.88	2.22	2.09	1.80

[a]For the definition of the atomic labels, see Figure 4.

interatomic distances given in this section were obtained using the B3LYP functional and, unless noted otherwise, the TZVP basis set as QM treatment in the DFT/CHARMM calculations. The specific atom labels used in the text are defined in Figure 4. Whenever necessary they will be specified in the format Resname:AtomName, for example FADO:OX3′ for atom OX3′ in $FADHOO^-$. Some characteristic interatomic distances in the stationary points along the reaction path are listed in Table 1.

3.1. Addition Step and Criegee Intermediate. In the optimized enzyme−reactant complex (Figure 4), cyclohexanone and $FADHOO^-$ are still far apart, with a distance of 3.41 Å between the carbonyl carbon of cyclohexanone (CYHN:C1) and the distal oxygen of the $FADHOO^-$ peroxy group (FADO:OX3′). As noted above, the cyclohexanone oxygen atom (CYHN:O1) is oriented toward hydrogen atoms at Arg-329 (H^{ε}) and the $NADP^+$ ribose 2′-hydroxyl group (NADP:HN2T). The corresponding distances (1.91 and 1.77 Å, respectively) are short and indicate hydrogen bonding. Otherwise cyclohexanone is surrounded by the hydrophobic residues of the binding pocket. One of the $NADP^+$ nicotinamide hydrogen atoms (NADP:HN71) forms a hydrogen bond with the proximal oxygen of the $FADHOO^-$ peroxy group (FADO:OX3) (1.88 Å), consistent with experimental

dx.doi.org/10.1021/ja2103839 | J. Am. Chem.Soc. 2012, 134, 2732−2741

evidence that $NADP^+$ stabilizes the C4a-peroxyflavin, while the distal oxygen of the $FADHOO^-$ peroxy group is close to the Arg-329 H^{η} atom (1.57 Å).

Starting from the optimized enzyme–reactant complex (Figure 4), a potential energy scan was performed for the addition step. The reaction coordinate was defined as the distance between the carbonyl carbon of cyclohexanone and the distal oxygen of the $FADHOO^-$ peroxy group, $d_{C1-OX3'}$, since there is a covalent bond between these atoms in the Criegee intermediate. During the scan, this distance was successively decreased in steps of 0.1 Å until the value of 1.6 Å was reached. The resulting QM/MM potential energy curve (see Figure 5 for QM = B3LYP/TZVP and SI, Figure S2 for QM = B3LYP/SVP) is relatively smooth, with a maximum of about 8.7 kcal/mol at $d_{C1-OX3'}$ close to 1.9 Å. Beyond this point, the energy goes down again because of the formation of the Criegee intermediate. There is some minor unevenness in the computed energy profile arising from the limited precision of the geometry optimizations, particularly with regard to structural features governed by weak non-covalent interactions.

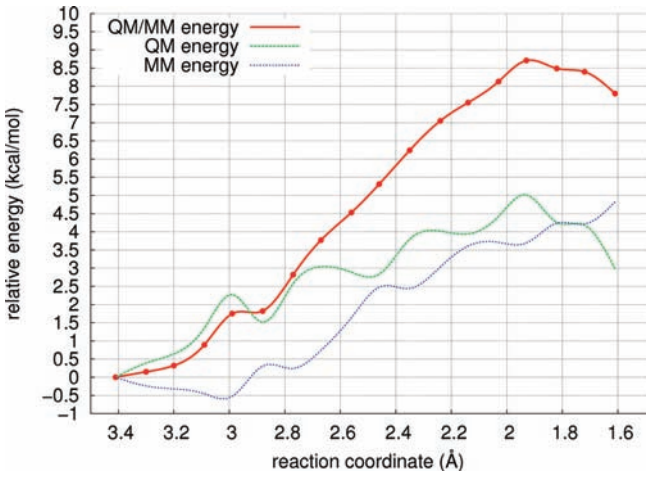

Figure 5. Energy profile for the addition step computed at the QM(B3LYP/TZVP)/CHARMM level using the reaction coordinate $d_{C1-OX3'}$.

Figure 5 also shows the decomposition of the QM/MM energy into QM and MM contributions (with the QM energy including the electrostatic interactions between QM atoms and MM point charges). The MM curve shows an overall rise, with some fluctuations (by typically less than 1 kcal/mol). Since all atoms directly involved in the formation of the Criegee intermediate are part of the QM region, and since there are no significant motions in the binding pocket during the scan (except for the cyclohexanone getting closer to the C4a-peroxyflavin peroxy group and undergoing a slight rotation), the rise of MM energy is probably due to the weakening of the van der Waals interactions between cyclohexanone and the active-site MM residues. The QM energy fluctuates around ~4 kcal/mol (relative to the reactant complex) at distances between 2.3 and 1.9 Å and then drops slightly. As a consequence of compensating changes in the QM and MM energies, the overall QM/MM energy profile is rather flat in this region, and a TS search starting from its highest point actually did not converge. The final point from the scan at a distance of 1.6 Å is only slightly lower in energy than the highest point, but when subjected to unconstrained minimization, it retains the covalent C1-OX3′ bond and yields the Criegee intermediate. During this minimization, the geometry changes only very slightly.

We also carried out single-point QM(B3LYP-D2/TZVP)/CHARMM calculations with empirical dispersion corrections at geometries taken from the QM(B3LYP/SVP)/CHARMM scan (see SI, Figure S3 for the energy profile) and at the corresponding optimized stationary points. In this case, the QM energy decreased from the reactant complex to the intermediate, with no intervening maximum, because of the inclusion of the attractive dispersion interactions. However, because of the concomitant increase in the MM energy, there is still a barrier such that unconstrained reoptimization of the reactant complex at the QM(B3LYP-D2/TZVP)/CHARMM level essentially retained its structure and did not produce the Criegee intermediate. Given the well-organized active site of CHMO, we did not consider it necessary to perform further reoptimizations at this level, thus assuming that the essential dispersion effects on the energy profile can be captured by single-point QM(B3LYP-D2/TZVP)/CHARMM calculations, in line with previous findings.[44]

In an attempt to follow the dynamics of the addition step, we performed QM/CHARMM MD simulations using the semi-empirical OM3 method for the QM part and starting from the reactant complex. After heating the system up to 300 K, the Criegee intermediate was formed spontaneously after about 3.5 ps and remained stable thereafter for the following 5.5 ps of the MD run. Figure 6 shows the variation of several key distances during the MD simulation. The distance $d_{C1-OX3'}$ fluctuates around 3.3 Å during the first 3.2 ps and then quickly shrinks to the covalent bond distance of 1.5 Å which is retained in the remaining time. These dynamics results suggest that there should exist a low-lying TS for the addition step at the OM3/CHARMM level. This TS could indeed be optimized properly on the OM3/CHARMM potential energy surface, as well as the reactant complex and the Criegee intermediate (see SI and Figure S4 for detailed results). The computed OM3/CHARMM barrier for the addition step is 5.7 kcal/mol, which is reasonably close to the value of about 8.7 kcal/mol obtained from the QM(B3LYP/TZVP)/CHARMM energy profile (Figure 5). Free energy calculations using thermodynamic integration lower the OM3/CHARMM barrier for

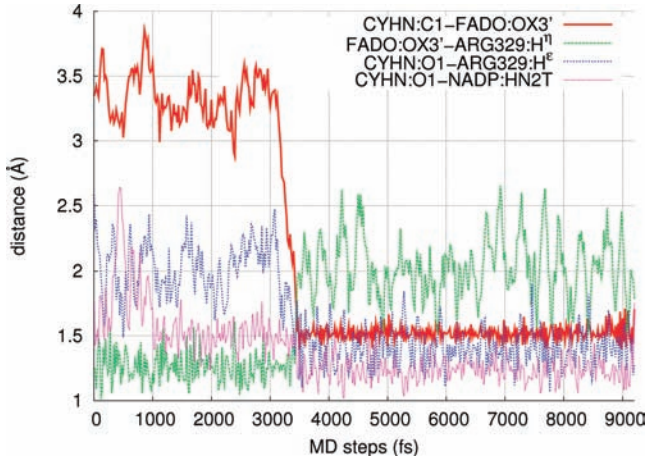

Figure 6. Changes in selected interatomic distances during the OM3/CHARMM MD simulation. For the definition of the atomic labels, see Figure 4.

dx.doi.org/10.1021/ja2103839 | J. Am. Chem.Soc. 2012, 134, 2732–2741

addition to 4.3 kcal/mol, thus making it feasible to directly observe this reaction in the OM3/CHARMM MD runs.

Contrary to previous theoretical work[17d] on the gas-phase acid-catalyzed B−V oxygenation of cyclohexanone, the carbonyl oxygen of cyclohexanone is not protonated in the Criegee intermediate within the enzyme (see Figure 7). However, it is

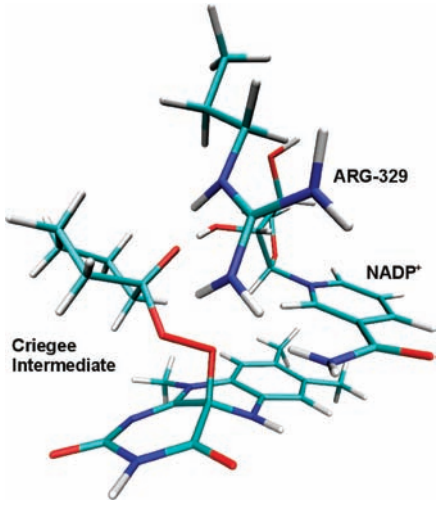

Figure 7. Criegee intermediate (QM region only) optimized at the QM(B3LYP/TZVP)/CHARMM level. For characteristic interatomic distances, see text and Table 1.

in close proximity to the hydrogen atoms at Arg-329 (H^{ε}, 1.60 Å) and the $NADP^+$ ribose 2′-hydroxyl group (1.53 Å). These two hydrogen bonds are strong enough to stabilize the intermediate and to make the carbonyl carbon atom more electrophilic. As a further check on the stability of the deprotonated Criegee intermediate, we performed a QM-(B3LYP/TZVP)/CHARMM potential energy scan for the proton transfer from Arg-329 to the carbonyl oxygen, using as reaction coordinate the difference of distances in the bonds being formed and broken, $d_{O1-H\varepsilon}-d_{H\varepsilon-N\varepsilon}$. The QM/MM energy was rising monotonously in this scan (up to 4.6 kcal/mol at the last point), indicating that this proton transfer does not occur spontaneously in the enzyme.

For reasons that will become clear when addressing the migration step (section 3.2), we also considered the alternative substrate binding mode (SI, Figure S1) and performed an OM3/CHARMM potential energy scan for the addition step leading to the respective Criegee intermediate. This turned out to be less favorable: in order to undergo nucleophilic C−O bond formation with the peroxy group, cyclohexanone must undergo an energetically costly conformational change such that the carbonyl oxygen atom points in the proper direction (i.e., the same as in the originally discussed approach, Figure 4). Importantly, the Criegee intermediate obtained in this manner contains cyclohexanone in a boat-like conformation and is 4.6 kcal/mol (OM3/CHARMM) higher in energy than the original one (Figure 7). It thus appears that the preferred binding mode of cyclohexanone generally involves an orientation as shown in Figure 4, and the energetically favored pathway will then be the one with cyclohexanone in its most stable chairlike conformation.

Our data support experimental evidence that $NADP^+$ and Arg-329 play a crucial role in stabilizing the C4a-peroxyflavin and the Criegee intermediate. In the initial phase of the addition reaction, there are strong hydrogen bonds between the nicotinamide hydrogen atom and the proximal oxygen of the $FADHOO^-$ peroxy group as well as between the 2′-hydroxyl group of the adjacent ribose group and the carbonyl oxygen of cyclohexanone. The latter stabilizing interaction is retained in the Criegee intermediate, whereas the former is diminished since the nicotinamide ring amino group shifts away (up to 2.2 Å) from the proximal oxygen of the $FADHOO^-$ peroxy group as soon as the intermediate is formed (probably due to the reduced nucleophilicity of the peroxy group).

3.2. Migration Step. In the Criegee intermediate arising from the energetically preferred orientation of cyclohexanone in the binding pocket, the C1−C2 bond of cyclohexanone is antiperiplanar to the peroxy bond of the C4a-peroxyflavin, with the FADO:OX3-OX3′-CYHN:C1−C2 dihedral angle being close to 180°. Because of the stereoelectronic requirement, the migration step of the B−V reaction is expected to involve a bond antiperiplanar to the peroxy bond.[45] Therefore a QM(B3LYP/SVP)/CHARMM potential energy scan was performed using as reaction coordinate the distance between the distal oxygen atom of the peroxy group and the C2 atom of cyclohexanone, $d_{OX3'-C2}$, which was successively decreased in steps of 0.05 Å until the value of 1.5 Å was reached. During this scan, the QM/MM energy of the system first rises fast and then at some point decreases dramatically (see SI, Figure S5). This sudden drop is associated with the insertion of the distal oxygen from the peroxy group into the cyclohexanone ring and the dissociation of the product from the isoalloxazine ring. The following smooth decrease of the QM/MM energy along the reaction coordinate reflects the gradual approach of the oxygen−carbon distance in the ε-caprolactone ring to its equilibrium value.

A TS search starting from the maximum-energy geometry was successful. In the resulting QM(B3LYP/TZVP)/CHARMM transition structure (see Figure 8), characteristic

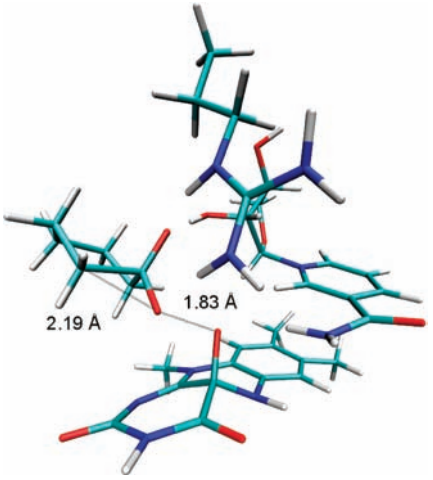

Figure 8. Transition state for the migration step (QM region only) optimized at the QM(B3LYP/TZVP)/CHARMM level. For characteristic interatomic distances, see Table 1.

distances are those between the two former peroxy group oxygen atoms (1.83 Å) and between the distal oxygen of the peroxy group and the C2 atom of cyclohexanone (2.19 Å). The energy barrier to migration is computed to be 6.7 kcal/mol at this level. To verify the type of TS, we distorted its geometry slightly along the transition vector in both directions and

dx.doi.org/10.1021/ja2103839 | J. Am. Chem.Soc. 2012, 134, 2732−2741

thereafter performed careful energy minimizations (with smaller maximum step sizes than usual) which led to the Criegee intermediate in one direction and the product (see Figure 9) in the other direction (as expected). The optimized

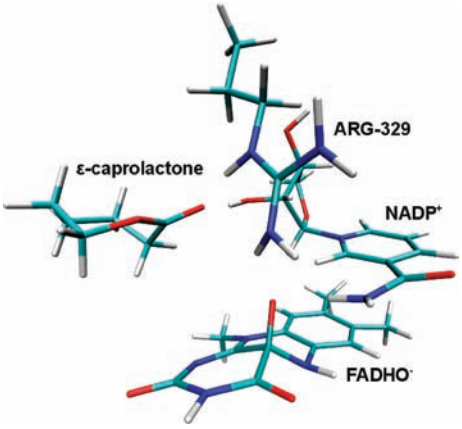

Figure 9. Enzyme–product complex (QM region only) optimized at the QM(B3LYP/TZVP)/CHARMM level. For characteristic interatomic distances, see Table 1.

enzyme–product complex is 81.4 kcal/mol lower in energy than the Criegee intermediate, and the overall reaction is highly exothermic with a reaction energy of −66.9 kcal/mol at the QM(B3LYP/TZVP)/CHARMM level. The overall energy profile is depicted in Figure 10, and the energies of all

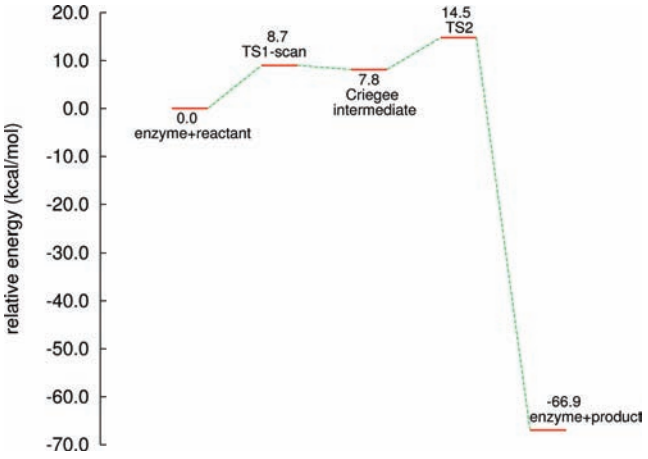

Figure 10. QM(B3LYP/TZVP)/CHARMM energy profile.

stationary points are given in Table 2 at different levels of theory. We note that the two QM approaches that include midrange dispersion (B3LYP-D2 and M06-2X) yield lower relative energies for the first transition state (TS1) and the Criegee intermediate (compared with B3LYP/TZVP). For the migration step (TS2), the barrier from QM(M06-2X/TZVP)/CHARMM is higher than that from QM(B3LYP/TZVP)/CHARMM, which may correct for the known general tendency of B3LYP to underestimate barriers; however, relative to the reactant complex, both approaches yield a similar energy for TS2 (14.3 vs 12.8 kcal/mol). Finally, all methods predict the overall enzymatic reaction to be very exothermic, with reaction energies between −66.5 and −70.4 kcal/mol.

To confirm that the migration step will preferably proceed as described (with the bond antiperiplanar to the peroxy bond being the one to migrate), another potential energy scan was performed, taking as reaction coordinate the distance between the distal oxygen of the peroxy group and the other carbon atom (C6) connected to the carbonyl carbon of cyclohexanone, $d_{OX3'-C6}$. The resulting QM(B3LYP/SVP)/CHARMM energy profile had a very high maximum of about 26 kcal/mol. Moreover, during a subsequent TS search, the distal oxygen from the peroxy group flipped, assuming an orientation close to the one adopted in the potential energy scan along the $d_{OX3'-C2}$ reaction coordinate. We thus conclude that the structure of the Criegee intermediate completely determines the preferred mode of migration. This implies that the energetically preferred binding mode of cyclohexanone (Figure 4) sets the stage for all subsequent molecular events. If the alternative binding mode (SI, Figure S1) were to be followed in the subsequent steps, then the other carbon atom (C6) would participate in the migration. Whereas C2 and C6 are equivalent by symmetry in the free cyclohexanone molecule, this is not so when it is complexed in the chiral binding pocket. As shown in section 3.5, this discrimination between C2 and C6 is crucial in determining the sense of stereoselectivity in the oxidative desymmetrization of **1**.

Table 2. Calculated QM/MM Energies (in kcal/mol) for Stationary Points along the Reaction Profile Relative to the Reactant Complex, Obtained with Different QM Methods

	reactant	TS1 scan	intermediate	TS2	product
B3LYP/SVP// B3LYP/SVP	0.0	3.6	0.8	9.3	−69.3
B3LYP/TZVP// B3LYP/SVP	0.0	7.9	7.6	14.3	−66.5
B3LYP/TZVP// B3LYP/TZVP	0.0	8.7	7.8	14.5	−66.9
B3LYP-D2/TZVP// B3LYP/SVP	0.0	−0.3	−4.0	3.4	−68.8
M06−2X/TZVP// B3LYP/SVP	0.0	1.7	−6.2	12.8	−70.4

3.3. Gas-Phase Calculations. Generally speaking, the protein environment in CHMO promotes the B–V reaction by defining the spatial orientation of the two cofactors and by properly placing the catalytic Arg-329 side chain within the active site. To check the influence of the MM region on the reaction mechanism in more detail, we performed pure QM gas-phase reoptimizations of the QM region for the relevant minima, transition states, and reaction paths at the B3LYP/TZVP level, starting from the corresponding QM/MM geometries. In these calculations, we (partially) retained the overall spatial arrangement within the QM region by keeping the Cartesian coordinates of all atoms fixed that are covalently bound to MM atoms in the QM/MM setup.

The most significant difference between the reactant complex in the gas phase and in the enzyme is a proton transfer from Arg-329 to $FADHOO^-$ that happens during the gas-phase reoptimization of the QM region. In the enzyme, Arg-329 is protonated (with a covalent H^{η}–N^{η} bond), and there is a short hydrogen bond between OX3′ and H^{η}, whereas in the gas-phase reoptimization, H^{η} quickly moves from N^{η} to the OX3′ atom in $FADHOO^-$ (with $d_{H^{\eta}-N^{\eta}}$ = 1.57 Å in the equilibrium structure). These gas-phase results are at odds with the experimental evidence for the enzyme where $FADHOO^-$ remains deprotonated in its active state. Apparently the protein environment stabilizes the deprotonated form of $FADHOO^-$ in the reactant complex, presumably via the two strong hydrogen

dx.doi.org/10.1021/ja2103839 | J. Am. Chem.Soc. 2012, 134, 2732–2741

bonds between Arg-329 and Asp-59 which make the nitrogen atoms of the arginine guanidinium group more nucleophilic. Furthermore, the overall geometry of the reactant complex changes substantially upon gas-phase reoptimization because the isoalloxazine and nicotinamide rings rotate (being repelled by each other) and reorient with respect to the cyclohexanone ring, such that the FADO:OX3-OX3′-CYHN:C1−C2 dihedral angle decreases from 170° to 100°; however, cyclohexanone remains hydrogen bonded via the carbonyl oxygen atom with Arg-329 (H^{ε}) and with the $NADP^+$ ribose 2′-hydroxyl group (which are part of the QM region).

The structure of the Criegee intermediate complex changes much less upon gas-phase reoptimization, and the Criegee intermediate itself remains deprotonated and retains its anionic character. The gas-phase reaction from the reactant to the intermediate thus requires significant conformational changes: to enable the formation of the covalent bond between CYHN:C1 and FADO:OX3′ the proton must first be transferred back to Arg-329:N^{η}, and in the Criegee intermediate the FADO:OX3-OX3′-CYHN:C1−C2 dihedral angle must be close to 180° (which is crucial for the reaction to proceed further). This causes the energy barrier for the addition step to be much higher (18 kcal/mol) than in the enzyme. The gas-phase Criegee intermediate lies 12 kcal/mol above the reactant complex, and hence 6 kcal/mol below the TS for its formation. The enzyme thus lowers the energy barrier for the addition step not only by constraining the spatial orientation of the cofactors, but also by allowing the cyclohexanone to be bound in a reactant conformation with the FADO:OX3-OX3′-CYHN:C1−C2 dihedral angle being close to 180° and by stabilizing the deprotonated form of the C4a-peroxyflavin.

The energy barrier for the migration step is also higher in the gas phase than in the enzyme (12 vs 6.7 kcal/mol) even though the corresponding TSs are geometrically not very different. For example, the key distances in the breaking OX3-OX3′ bond and the forming OX3′−C2 bond are 1.93 and 2.17 Å in the gas-phase TS (compared with 1.83 and 2.19 Å in the enzyme, respectively), and it is thus difficult to pinpoint geometrical factors that would account for the lower barrier in the enzyme. The overall reaction energies are rather similar in the gas phase and in the enzyme (−64 vs −66.9 kcal/mol).

3.4. Comparison with Reaction in Solution. According to our calculations, the mechanism of the CHMO-catalyzed B−V oxidation of cyclohexanone differs from that of the acid-catalyzed reaction in solution that has been described previously.[17d] In the latter case, the presence of a strong acid like trifluoroacetic acid (TFAA) causes protonation of the carbonyl oxygen during the addition step, which increases the electrophilicity of the carbonyl carbon atom and thus facilitates the addition of the peroxyacid (which is at the same time deprotonated by the same TFA that protonates the substrate in a concerted fashion).[17d] Hence this acid-catalyzed solution reaction generates a neutral Criegee intermediate, contrary to the situation in the enzyme where, according to our QM/MM calculations, the carbonyl oxygen is not protonated although doubly H-bonded, and the Criegee intermediate has pronounced anionic character. We note in this context that both the protonated arginine and the hydroxyl group are weak acids with pK_a values higher than 10 and that the hydrogen bonds, which they form in CHMO with the carbonyl oxygen, seem strong enough to make the carbonyl carbon sufficiently electrophilic. As mentioned elsewhere,[16] the anionic nature of the Criegee intermediate is expected to accelerate the migration step, and one important role of the enzyme is thus the effective stabilization of this kind of Criegee adduct, which allows for a faster overall reaction compared with an acidic solution.

3.5. Unveiling the Source of Enantioselectivity of CHMO. After exploring the mechanism of the CHMO-catalyzed B−V reaction for the parent substrate cyclohexanone, we now turn to a substituted substrate, namely **1**, and study the stereoselectivity of its reaction. It is experimentally known that CHMO (*Rhodococcus*) as well as CHMO (*Acinetobacter*) react with this substrate with nearly perfect (*S*)-enantioselectivity providing (*S*)-**2** with >96% ee (Figure 2). Chemists have long speculated about the source of enantioselectivity in BVMO-catalyzed transformations (including the asymmetric **1** → **2** transformation).[5,46,47] The traditional stereoelectronic requirement regarding anti-periplanarity in the cleavage (fragmentation) of the Criegee intermediate, known to be essential in nonenzymatic reactions, formed a common basis in all attempts to develop a model. Then, upon considering the empirical results of BVMO-catalyzed asymmetric transformations of numerous cyclohexanone derivatives, appropriate models were proposed by Furstoss,[46a] Ottolina and Colonna,[46b] Kelly,[46c] Stewart,[46d,47] and Kayser.[5,7] Especially the "diamond lattice model", in which the substrate is assumed to have the chair conformation with substituents in the equatorial position, has proven to be a useful mnemonic aid with notable predictive power.[5,7,46d,47] We are now in the position to deliver the underlying explanation for these models on the molecular level. Making the reasonable assumption that the 4-methyl group adopts the equatorial position in the cyclohexanone chair conformation in the preferred binding mode (Figure 4), our optimized structure of the Criegee intermediate (Figure 7) immediately suggests exclusive formation of the (*S*)-lactone product by energetically favored selective migration of C2 rather than C6.

To verify this qualitative prediction, we have built the two 4-methyl-substituted Criegee intermediates by manually adding a methyl group into the optimized geometry of the original Criegee intermediate. The resulting structures were fully reoptimized at the QM(B3LYP/TZVP)/CHARMM level, followed by energy scans and TS searches for the migration step. As expected, the energies of the Criegee intermediate and the TS are lower when an equatorial rather than an axial 4-methyl group is present, by 4.8 and 4.5 kcal/mol, respectively. For an isolated molecule of **1**, gas-phase B3LYP/TZVP calculations favor the equatorial over the axial conformer by 1.9 kcal/mol (energy difference including zero-point vibrational corrections), close to the experimental value of 2.1 kcal/mol for the enthalpy difference between the two conformers.[48] The preference for the equatorial form is thus reinforced both in the Criegee intermediate and the subsequent TS in CHMO. While the energy barriers to migration are quite similar within each conformer, the equatorial pathway is favored overall by an energy difference of 4.5 kcal/mol at the crucial TS, and hence the (*S*)-lactone product will be formed with high enantioselectivity.

Our current mechanistic scenario for the mechanism of the CHMO-catalyzed B−V reaction thus reproduces and explains on a molecular level the observed (*S*)-enantioselectivity for the chiral substrate **1** very well. This pertains to CHMO (*Rhodococcus*) and other homologous CHMOs such as the most used CHMO (*Acinetobacter*). On this basis it should thus be possible to make qualitative predictions concerning the enantioselectivity for other substituted cyclohexanone deriva-

dx.doi.org/10.1021/ja2103839 | J. Am. Chem.Soc. 2012, 134, 2732−2741

tives and the effect of active-site mutations. One such example is the B−V oxidation of 4-hydroxycyclohexanone by CHMO (*Acinetobacter*) which changes from marginal (*R*)-enantioselectivity (9% ee) in the wild-type enzyme to good (*S*)-enantioselectivity (79% ee) in the Phe432Ser mutant.[7] Our model immediately suggests an explanation for this drastic change in terms of the orientation of the substrate in the binding site and the formation of a hydrogen bond in the mutant between Ser432 and the 4-hydroxy group of the substrate, which will lead to more favorable binding when the latter is in an equatorial rather than an axial position. We are currently studying the B−V oxidation of this substrate by QM/MM calculations to confirm the qualitative conclusions derived from our model and to arrive at quantitative assessments. The results of this work will be reported elsewhere.

4. CONCLUSION

We have reported the first computational investigation of the Baeyer−Villiger reaction proceeding in a native enzyme environment. Reaction pathways for cyclohexanone oxidation by cyclohexanone monooxygenase from *Rhodococcus* (CHMO) were determined as well as the structures of the Criegee intermediate and the transition states. Judging from the QM(B3LYP/TZVP)/CHARMM results, the initial addition reaction has to overcome an energy barrier of about 8.7 kcal/mol, which generates the Criegee intermediate that occupies a shallow minimum on the potential energy surface and can rearrange to the lactone product by surmounting a second energy barrier of 6.7 kcal/mol. The latter transition state for the migration step is the highest point on the energy profile. The CHMO-catalyzed reaction proceeds via a Criegee intermediate of anionic character and is highly exothermic, with a computed overall reaction energy of −66.9 kcal/mol. The QM/MM calculations confirm the crucial role of the Arg-329 residue and the $NADP^+$ cofactor for the catalytic efficiency of CHMO. The experimentally observed enantioselectivity toward **1** with essentially complete formation of the lactone (*S*)-**2** has been rationalized for the first time on a molecular basis by the current QM/MM calculations. It is the selective binding mode of the substrate in the chair conformation with the methyl-substituent in the equatorial position that places it in a chiral environment in a way that only one of the two enantiotopic C-atoms can migrate. This physical model also serves as a guide for interpreting the stereochemical results of other synthetically interesting transformations catalyzed by CHMO and other homologues such as the most used CHMO from *Acinetobacter* sp. NCIMB 9871.[4] Finally, this work provides insight into the possible effects of mutations aimed at tuning the enantio- and regioselectivity of CHMO and other BVMOs by rational design or directed evolution.[6−8]

■ ASSOCIATED CONTENT

Supporting Information

Figure of reactant complex with different substrate orientation, additional energy profiles, detailed results from OM3/CHARMM molecular dynamics, sequence alignment of CHMO (*Rhodococcus*) and CHMO (*Acinetobacter*), and complete refs 21 22b, and 29. This material is available free of charge via the Internet at http://pubs.acs.org.

■ AUTHOR INFORMATION

Corresponding Author

thiel@mpi-muelheim.mpg.de

■ ACKNOWLEDGMENTS

The authors thank Prof. Albert M. Berghuis for providing the Cartesian coordinates of their X-ray structure[14] before depositing them (PDB code 3GWD).

■ REFERENCES

(1) Baeyer, A.; Villiger, V. *Ber. Dtsch. Chem. Ges.* **1899**, *32*, 3625−3633.

(2) (a) Bolm, C.; Schlingloff, G.; Weickhardt, K. *Angew. Chem., Int. Ed. Engl.* **1994**, *33*, 1848−1849. (b) Gusso, A.; Baccin, C.; Pinna, F.; Strukul, G. *Organometallics* **1994**, *13*, 3442−3451. (c) Strukul, G. *Angew. Chem., Int. Ed.* **1998**, *37*, 1199−1209. (d) Uchida, T.; Katsuki, T. *Tetrahedron Lett.* **2001**, *42*, 6911−6914. (e) Ito, K.; Ishii, A.; Kuroda, T.; Katsuki, T. *Synlett* **2003**, 643−646. (f) Frison, J.-C.; Palazzi, C.; Bolm, C. *Tetrahedron* **2006**, *62*, 6700−6706. (g) Colladon, M.; Scarso, A.; Strukul, G. *Synlett* **2006**, 3515−3520.

(3) (a) Murahashi, S.; Ono, S.; Imada, Y. *Angew. Chem., Int. Ed.* **2002**, *41*, 2366−2368. (b) Imada, Y.; Iida, H.; Murahashi, S.; Naota, T. *Angew. Chem., Int. Ed.* **2005**, *44*, 1704−1706. (c) Wang, B.; Shen, Y.-M.; Shi, Y. *J. Org. Chem.* **2006**, *71*, 9519−9521. (d) Peris, G.; Miller, S. J. *Org. Lett.* **2008**, *10*, 3049−3052. (e) Malkov, A. V.; Friscourt, F.; Bell, M.; Swarbrick, M. E.; Kocovsky, P. *J. Org. Chem.* **2008**, *73*, 3996−4003. (f) Xu, S.; Wang, Z.; Zhang, X.; Zhang, X.; Ding, K. *Angew. Chem., Int. Ed.* **2008**, *47*, 2840−2843.

(4) For reviews see: (a) Mihovilovic, M.; Muller, B.; Stanetty, P. *Eur. J. Org. Chem.* **2002**, 3711−3730. (b) Wohlgemuth, R. *Eng. Life Sci.* **2006**, *6*, 577−583. (c) Rehdorf, J.; Bornscheuer, M. *Monooxygenases, Baeyer Villiger Applications in Organic Synthesis*; John Wiley & Sons: Hoboken, NJ, 2009. (d) de Gonzalo, G.; Mihovilovic, M. D.; Fraaije, M. W. *ChemBioChem* **2010**, *11*, 2208−2231. (e) Pazmino, D. E. T.; Dudek, H. M.; Fraaije, M. W. *Curr. Opin. Chem. Biol.* **2010**, *14*, 138−144. (f) Leisch, H.; Morley, K.; Lau, P. *Chem. Rev.* **2011**, *111*, 4165−4222.

(5) Kayser, M. M. *Tetrahedron* **2009**, *65*, 947−974.

(6) Review of directed evolution of enantioselective enzymes as catalysts in organic chemistry: Reetz, M. T. *Angew. Chem., Int. Ed.* **2011**, *50*, 138−174.

(7) Kayser, M. M.; Clouthier, C. M. *J. Org. Chem.* **2006**, *71*, 8424−8430.

(8) (a) Reetz, M.; Brunner, B.; Schneider, T.; Schulz, F.; Clouthier, C.; Kayser, M. *Angew. Chem., Int. Ed.* **2004**, *43*, 4075−4078. (b) Bocola, M.; Schulz, F.; Leca, F.; Vogel, A.; Fraaije, M.; Reetz, M. *Adv. Synth. Catal.* **2005**, *347*, 979−986. (c) Mihovilovic, M.; Rudroff, F.; Winninger, A.; Schneider, T.; Schulz, F.; Reetz, M. *Org. Lett.* **2006**, *8*, 1221−1224. (d) Clouthier, C. M.; Kayser, M. M.; Reetz, M. T. *J. Org. Chem.* **2006**, *71*, 8431−8437. (e) Reetz, M. T.; Wu, S. *J. Am. Chem. Soc.* **2009**, *131*, 15424−15432. (f) Wu, S.; Acevedo, J. P.; Reetz, M. T. *Proc. Natl. Acad. Sci. U.S.A.* **2010**, *107*, 2775−2780. (g) Kirschner, A.; Bornscheuer, U. T. *Angew. Chem., Int. Ed.* **2006**, *45*, 7004−7006. (h) Kirschner, A.; Bornscheuer, U. T. *Appl. Microbiol. Biotechnol.* **2008**, *81*, 465−472. (i) Rehdorf, J.; Mihovilovic, M. D.; Bornscheuer, U. T. *Angew. Chem., Int. Ed.* **2010**, *49*, 4506−4508.

(9) (a) Turfitt, G. *Biochem. J.* **1948**, *42*, 376−383. (b) Donoghue, N.; Norris, D.; Trudgill, P. *Eur. J. Biochem.* **1976**, *63*, 175−192. (c) Chen, Y.; Peoples, O.; Walsh, C. *J. Bacteriol.* **1988**, *170*, 781−789.

(10) (a) Ryerson, C.; Ballou, D.; Walsh, C. *Biochemistry* **1982**, *21*, 2644−2655. (b) Walsh, C.; Chen, Y. *Angew. Chem., Int. Ed. Engl.* **1988**, *27*, 333−343. (c) Brzostowicz, P.; Walters, D.; Thomas, S.; Nagarajan, V.; Rouviere, P. *Appl. Environ. Microbiol.* **2003**, *69*, 334−342.

(11) Sheng, D.; Ballou, D.; Massey, V. *Biochemistry* **2001**, *40*, 11156−11167.

(12) Pazmino, D. E. T.; Baas, B.-J.; Janssen, D. B.; Fraaije, M. W. *Biochemistry* **2008**, *47*, 4082−4093.

(13) Orru, R.; Dudek, H. M.; Martinoli, C.; Pazmino, D. E. T.; Royant, A.; Weik, M.; Fraaije, M. W.; Mattevi, A. *J. Biol. Chem.* **2011**, *286*, 29284−29291.
(14) Mirza, I. A.; Yachnin, B. J.; Wang, S.; Grosse, S.; Bergeron, H.; Imura, A.; Iwaki, H.; Hasegawa, Y.; Lau, P. C. K.; Berghuis, A. M. *J. Am. Chem. Soc.* **2009**, *131*, 8848−8854.
(15) Renz, M.; Meunier, B. *Eur. J. Org. Chem.* **1999**, 737−750.
(16) ten Brink, G.; Arends, I.; Sheldon, R. *Chem. Rev.* **2004**, *104*, 4105−4123.
(17) (a) Okuno, Y. *Chem.—Eur. J.* **1997**, *3*, 212−218. (b) Grein, F.; Chen, A.; Edwards, D.; Crudden, C. *J. Org. Chem.* **2006**, *71*, 861−872. (c) Alvarez-Idaboy, J.; Reyes, L.; Cruz, J. *Org. Lett.* **2006**, *8*, 1763−1765. (d) Alvarez-Idaboy, J. R.; Reyes, L.; Mora-Diez, N. *Org. Biomol. Chem.* **2007**, *5*, 3682−3689. (e) Alvarez-Idaboy, J. R.; Reyes, L. *J. Org. Chem.* **2007**, *72*, 6580−6583. (f) Mora-Diez, N.; Keller, S.; Alvarez-Idaboy, J. R. *Org. Biomol. Chem.* **2009**, *7*, 3682−3690.
(18) Malito, E.; Alfieri, A.; Fraaije, M.; Mattevi, A. *Proc. Natl. Acad. Sci. U.S.A.* **2004**, *101*, 13157−13162.
(19) (a) Gordon, J.; Myers, J.; Folta, T.; Shoja, V.; Heath, L.; Onufriev, A. *Nucleic Acids Res.* **2005**, *33*, W368−W371. (b) Anandakrishnan, R.; Onufriev, A. *J. Comp. Biol.* **2008**, *15*, 165−184.
(20) Li, H.; Robertson, A.; Jensen, J. *Proteins* **2005**, *61*, 704−721.
(21) MacKerell, A.; et al. *J. Phys. Chem. B* **1998**, *102*, 3586−3616.
(22) (a) Brooks, B.; Bruccoleri, R.; Olafson, D.; States, D.; Swaminathan, S.; Karplus, M. *J. Comput. Chem.* **1983**, *4*, 187−217. (b) Brooks, B. R.; et al. *J. Comput. Chem.* **2009**, *30*, 1545−1614.
(23) Morris, G. M.; Goodsell, D. S.; Halliday, R. S.; Huey, R.; Hart, W. E.; Belew, R. K.; Olson, A. J. *J. Comput. Chem.* **1998**, *19*, 1639−1662.
(24) Warshel, A.; Levitt, M. *J. Mol. Biol.* **1976**, *103*, 227−249.
(25) Senn, H. M.; Thiel, W. *Angew. Chem., Int. Ed.* **2009**, *48*, 1198−1229.
(26) (a) Slater, J. *Phys. Rev.* **1953**, *91*, 528−530. (b) Vosko, S.; Wilk, L.; Nusair, M. *Can. J. Phys.* **1980**, *58*, 1200−1211. (c) Becke, A. *Phys. Rev. A* **1988**, *38*, 3098−3100. (d) Becke, A. *J. Chem. Phys.* **1993**, *98*, 5648−5652. (e) Stephens, P.; Devlin, F.; Chabalowski, C.; Frisch, M. *J. Phys. Chem.* **1994**, *98*, 11623−11627. (f) Lee, C.; Yang, W.; Parr, R. *Phys. Rev. B* **1988**, *37*, 785−789.
(27) Bakowies, D.; Thiel, W. *J. Phys. Chem.* **1996**, *100*, 10580−10594.
(28) (a) de Vries, A.; Sherwood, P.; Collins, S.; Rigby, A.; Rigutto, M.; Kramer, G. *J. Phys. Chem. B* **1999**, *103*, 6133−6141. (b) Sherwood, P.; de Vries, A.; Collins, S.; Greatbanks, S.; Burton, N.; Vincent, M.; Hillier, I. *Farad. Disc.* **1997**, *106*, 79−92.
(29) Sherwood, P.; et al. *J. Mol. Struct. (Theochem)* **2003**, *632*, 1−28.
(30) Ahlrichs, R.; Bär, M.; Häser, M.; Horn, H.; Kölmel, C. *Chem. Phys. Lett.* **1989**, *162*, 165−169.
(31) Smith, W.; Forester, T. *J. Mol. Graph.* **1996**, *14*, 136−141.
(32) Billeter, S.; Turner, A.; Thiel, W. *Phys. Chem. Chem. Phys.* **2000**, *2*, 2177−2186.
(33) Kästner, J.; Carr, J. M.; Keal, T. W.; Thiel, W.; Wander, A.; Sherwood, P. *J. Phys. Chem. A* **2009**, *113*, 11856−11865.
(34) Schäfer, A.; Horn, H.; Ahlrichs, R. *J. Chem. Phys.* **1992**, *97*, 2571−2577.
(35) Schäfer, A.; Huber, C.; Ahlrichs, R. *J. Chem. Phys.* **1994**, *100*, 5829−5835.
(36) Grimme, S. *J. Comput. Chem.* **2006**, *27*, 1787−1799.
(37) Zhao, Y.; Truhlar, D. G. *Theor. Chem. Acc.* **2008**, *120*, 215−241.
(38) (a) Nocedal, J. *Math. Comp.* **1980**, *35*, 773−782. (b) Liu, D.; Nocedal, J. *Math. Programming* **1989**, *45*, 503−528.
(39) (a) Banerjee, A.; Adams, N.; Simons, J.; Shepard, R. *J. Phys. Chem.* **1985**, *89*, 52−57. (b) Baker, J. *J. Comput. Chem.* **1986**, *7*, 385−395.
(40) (a) Nose, S. *J. Chem. Phys.* **1984**, *81*, 511−519. (b) Hoover, W. *Phys. Rev. A* **1985**, *31*, 1695−1697.
(41) (a) Scholten, M. Ph.D. thesis, Universität Düsseldorf, 2003. (b) Otte, N.; Scholten, M.; Thiel, W. *J. Phys. Chem. A* **2007**, *111*, 5751−5755.
(42) Ryckaert, J.; Ciccotti, G.; Berendsen, H. *J. Comput. Phys.* **1977**, *23*, 327−341.
(43) Senn, H. M.; Thiel, S.; Thiel, W. *J. Chem. Theory Comput.* **2005**, *1*, 494−505.
(44) Lonsdale, R.; Harvey, J. N.; Mulholland, A. J. *J. Phys. Chem. Lett.* **2010**, *1*, 3232−3237.
(45) Krow, G. *Tetrahedron* **1981**, *37*, 2697−2724.
(46) (a) Alphand, V.; Furstoss, R. *J. Org. Chem.* **1992**, *57*, 1306−1309. (b) Ottolina, G.; Carrea, G.; Colonna, S.; Rückemann, A. *Tetrahedron: Asymmetry* **1996**, *7*, 1123−1136. (c) Kelly, D. R. *Tetrahedron: Asymmetry* **1996**, *7*, 1149−1152. (d) Stewart, J. *Curr. Org. Chem.* **1998**, *2*, 195−216.
(47) Stewart, J.; Reed, K.; Martinez, C.; Zhu, J.; Chen, G.; Kayser, M. *J. Am. Chem. Soc.* **1998**, *120*, 3541−3548.
(48) Potts, A.; Baer, T. *J. Mol. Struct. (Theochem)* **1997**, *419*, 11−18.